Journal of the Iranian Chemical Society
https://doi.org/10.1007/s13738-020-02082-y

ORIGINAL PAPER

Effect of different acceptors on *N*-hexyl carbazole moiety for dye-sensitized solar cells: design, characterization, molecular structure, and DSSC fabrications

Moustafa S. Abusaif[1] · M. A. Abu-Saied[2] · M. Fathy[3] · Ahmed A. El-Sherif[4] · A. B. Kashyout[3] · Mohamed R. Selim[1] · Yousry A. Ammar[1]

Received: 18 July 2020 / Accepted: 30 September 2020

Abstract

Hexyl carbazole derivatives are one of the most prominent dye scaffolds in the dye-sensitized solar cells (DSSCs). New substituted carbazole dyes such as DRA-HC, DCA-HC, and DTC-HC were synthesized for DSSCs. These dyes are containing hexyl moiety as electron donor and rhodanine-3-acetic acid, cyanoacetic acid and tetracyanoethylene as an electron acceptor linked to carbazole moiety. The relation between dye structures, photophysical/electrochemical, molecular structure and DSSC manufacturing had been discussed. All structures showed more positive ground-state oxidation potential than I^-/I^-_3 and more negative excited state oxidation potential than the conduction band edge of the semiconductor. The highest efficiency of the DSSCs was obtained in the case of DCA-HC dye ($\eta = 1.41\%$, $V_{OC} = 708$ mV, FF = 0.81, and $J_{SC} = 2.45$ mA cm^{-2} with 100 mW cm^{-2}) compared to other synthesized dyes.

Keywords *N*-hexyl carbazole · Photovoltaic performance · DSSCs fabrication · Optical and electrochemical · Properties · Rhodanine-3-acetic acid

Abbreviations

DRA-HC	2,2′-(((9-Hexyl-9H-carbazole-3,6-diyl) bis(methanylylidene))bis(4-oxo-2-thioxothiazolidin-3-yl-5-ylidene))diacetic acid
DCA-HC	3-(6-(2-Carboxy-2-cyanovinyl)-9-hexyl-9H-carbazol-3-yl)-2-cyanoacrylic acid
DTC-HC	2,2′-((((9-Hexyl-9H-carbazole-3,6-diyl) bis(methanylylidene))bis(hydrazin-1-yl-2-ylidene))bis(4,1-phenylene)) bis(ethene-1,1,2-tricarbonitrile)
DSSCs	Dye-sensitized solar cells
V_{OC}	Open-circuit voltage
J_{SC}	Short-circuit current density
D–π–A	Donor–(π-conjugated spacer)–acceptor
TCNE	Tetracyanoethylene
TLC	Thin-layer chromatography
KBr	Potassium bromide
SEM	Scanning electron microscopy
CV	Cyclic voltammetry techniques
TBP	4-Tertbutylpyridine
ε	Molar absorptivity
E_{0-0}	Band gap
E_{LUMO}	Lowest unoccupied molecular orbital
τe	Electron lifetime

Electronic supplementary material The online version of this article (https://doi.org/10.1007/s13738-020-02082-y) contains supplementary material, which is available to authorized users.

✉ Ahmed A. El-Sherif
aelsherif72@yahoo.com

[1] Department of Chemistry, Faculty of Science, Al-Azhar University, Nasr City, Cairo, Egypt

[2] Polymeric Materials Research Department, Advanced Technology and New Materials Research Institute, City of Scientific Research and Technological Applications (SRTA-City), New Borg El-Arab City, Alexandria 21934, Egypt

[3] Electronic Materials Department, Advanced Technology and New Materials Research Institute, City of Scientific Research and Technological Applications (SRTA-City), New Borg El-Arab City, Alexandria 21934, Egypt

[4] Department of Chemistry, Faculty of Science, Cairo University, Giza, Egypt

Published online: 16 October 2020

IP	Ionization potential
η	Absolute hardness
ω	Electrophilicity index
ΔE	Separation energy
S	Global softness
η	Power conversion efficiency
FF	Fill factor
TiO_2	Titanium dioxide
ICT	Intermolecular charge transfer
TBAI	Tetra-*n*-butylammonium iodide
DMSO-d_6	Deuterated dimethyl sulfoxide
UV–Vis	Ultraviolet–visible
EIS	Electrochemical impedance spectroscopy
FTO	Fluorine-doped tin oxide
DMF	Dimethyl formamide
E_{ox}	Redox potentials
E_{HOMO}	Highest occupied molecular orbital
J–V	Current–voltage density
TMS	Tetra-methyl silane
σ	Absolute softness
EA	Electron affinity
ΔN_{max}	Maximum amount of electron transfer
χ	Absolute electronegativity

Introduction

No doubt that solar energy is widely recognized as a promising energy source that can contribute to the alleviation of the global energy crisis; the development of solar cells is a key research goal [1]. There are many types of solar cells such as silicon solar cell [2], organic solar cell (OPV) [3], perovskite solar cell [4], plasmonic solar cell [5], quantum dot solar cell [6], and dye-sensitized solar cell (DSSCs) [7]. Dye-sensitized solar cells (DSSCs) have arisen as a technically and economically credible alternative to the p–n junction photovoltaic devices [8]. Due to the advantages of the DSSCs, such as easy processing, low cost, ecologically friendly, and long-term durability, DSSCs are great alternative to silicon solar cells [9]. The sensitizers are usually designed to have functional groups such as –COOH, $–PO_3H_2$, and $–B(OH)_2$ for stable adsorption onto the semiconductor substrate [10]. Much of the current research focuses on improving the range of spectral absorbance by modifying the dye [11], on improving hole transport and cell stability by replacing the liquid electrolyte with ionic solids or conducting polymers and on improving electron transport by using alternative wide-band-gap semiconductor materials or core–shell structures [12]. Recently in 2018, an efficiency of up to 14.3% was achieved by Sharma et al. [13].

In general, there are two main kinds of sensitizers, metal-complex and organic metal-free sensitizers. However, the DSSCs based on metal-complex sensitizers as Ru complex have gained high conversion efficiency [14, 15], they are inefficient for large-scale applications due to their difficult preparation and the Ru atom is seldom and costly. For this cause, metal-free dyes have become more important when opposed to metal complexes because of their high and low cost, molecular extinction. In DSSCs, many types of sensitizers, including carbazole [16], coumarin [17], phenothiazine [18], indoline [19], are introduced in the literature as sensitizers for efficiency improvement. In general, sensitizers are made up of donor–π-conjugated spacer–acceptor (D–π–A) structure because of the efficacy photoinduced intermolecular charge transfer (ICT) property [20]. Carbazole moiety acts as donor linked to acceptor groups such as thiobarbituric acid has shown better light conversion efficiency similar to phenothiazine moieties due to carbazole containing a heterocyclic atom [21].

In this study, we report the synthesis of three novel metal-free organic dyes with a structure of (D–π–A) DRA-HC, DCA-HC, and DTC-HC (Fig. 1). In the design of these dyes, *N*-hexyl carbazole was used as the donor part, while rhodanine-3-acetic acid, cyanoacetic acid, and tetracyano ethylene were used as the withdrawal group in DRA-HC, DCA-HC, and DTC-HC, respectively. The effects on photophysical, electrochemical, and photovoltaic properties of these dyes were studied.

Experimental

Instrumentation and characterizations

For chromatographic isolation, Merck silica gel (254 nm plates) was used. The Gallen Kamp MFB-595 device is used to record all melting points. For the IR spectrum (KBr, cm^{-1}), a Shimadzu 440 was used. The Bruker spectrometers were used in deuterated dimethyl sulfoxide (DMSO-d_6) to investigate ^{1}H NMR and ^{13}C NMR spectra using TMS as standard. Mass spectrum is measured by the Thermo Scientific ISQLT Spectrometer. UV–Vis spectra have been registered on the Shimadzu 260 solution spectrometer. The particle size of the organic dyes was analyzed with a micrometer particle size analyzer (Beckman Coulter, USA). The sample, dispersed in water at 20 °C, had a viscosity of 1.002 and a refractive index of 1.33. The organic materials are investigated with high-resolution scanning electron microscopy (JEOL, JSM-6360LA) to examine the morphology and the homogeneity of the surface.

The recording of cyclic voltammograms was reported with the AUTOLAB potentiostat/galvanostat operated device and traditional three-electrode devices at room temperature, platinum working electrode, Ag/AgCl reference electrode and carbon counter electrode. The potential is recorded versus ferrocene as standard using

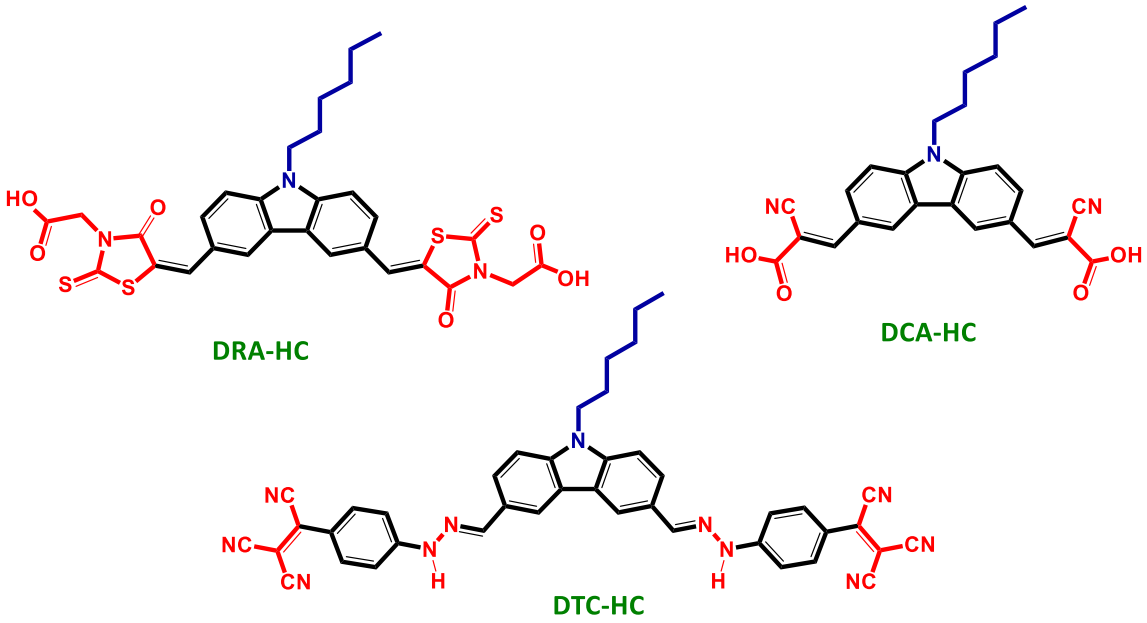

Fig. 1 Molecular structure of organic dyes

tetrabutylammonium iodide as supporting electrolyte and scan rate of 0.1 Vs^{-1} and 0.1 M.

Materials and synthesis

The starting material 9H-carbazole was purchased from Aldrich. The reagents such as rhodanine-3-acetic acid, cyanoacetic acid, phenylhydrazine, and tetracyanoethylene [TCNE] were purchased from Aldrich Chemicals. All organic solvents were obtained from Fisher and used without further purification. Also, literature process used was to prepare 9-hexyl-9H-carbazole 1, and 9-hexyl- 9H-carbazole-3,6-diformaldehyde 2, with melting point mp. = 75–77 °C and 79–80 °C, respectively [22, 23].

9-Hexyl-3,6-bis((2-phenylhydrazono) methyl)-9H-carbazole [3]

N-hexylcarbazole-3,6-dicarbaldehyde 2 (0.30 g, 1 mmol) and phenylhydrazine (0.21 g, 2 mmol) were added to absolute ethanol (10 ml), catalyzed with acetic acid (1 ml), and heated under reflux for 5 h until the precipitate is formed, and the reaction was monitored by TLC. The collected powders were dried, ethanol-washed, and acetic acid-recrystallized.

Yellow solid; 93% yield; mp: 185–187 °C; IR: ν/cm^{-1}: 3302 (NH), 3053 (arom. C–H), 2927, 2856 (alip. C–H), 1598 (C=N), 1488 (C–N); ^{1}H NMR: δ/ppm: 10.18, 10.24 (*s*, 2H, NH; D_2O exchangeable); 8.83 (*s*, 1H, H_4); 8.40 (*s*, 1H, H_5); 8.04 (*s*, 2H, methine-H); 7.83 (*d*, 1H, H_7), 7.62 (*d*, 1H, H_1), 6.70–7.60 (m, 12H, arom. C–H); 4.43 (t, 2H, N–CH_2); 1.77 (m, 2H, CH_2), 1.25 (m, 6H, CH_2), 0.79 (t, 3H, CH_3); ^{13}CNMR: δ 146.15 (alip. CH=N), 140.83, 138.36, 129.52, 127.77, 124.05, 123.60, 122.73, 122.09, 119.01, 118.69, 118.65, 112.29, 111.80, 110.33, 43.33 (N–CH_2), 31.05, 28.76, 26.55, 22.46, 14.43 (CH_3); Anal. Calcd. for $C_{32}H_{33}N_5$ (487.27): C, 78.82; H, 6.82; N, 14.36; Found: C, 78.45; H, 6.65; N, 14.30%.

2′-((((9-hexyl-9H-carbazole-3,6-diyl)bis(methanylylidene)) bis(hydrazin-1-yl-2-ylidene))bis(4,1-phenylene)) bis(ethene-1,1,2-tricarbonitrile) [DTC-HC]

To a solution of phenyl hydrazone derivatives 3 (0.68 g, 1 mmol) in DMF (20 ml), then TCNE (0.25 g, 2 mmol) was added, a dark color appeared. The solution boiled at 400 °C for 8 h, the solvent was removed, and the residual solid was collected and recrystallized from toluene-producing DTC-HC.

Red-brown solid; 60% yield; mp: 230–232 °C; IR: ν/cm^{-1}: 3319 (br. NH), 3059 (arom. C–H), 2929, 2858 (alip. C–H), 2216 (C≡N), 1604 (C=N), 1558 (C=C), 1489 (C–N); ^{1}H NMR: δ/ppm: 10.18, 10.24 (*s*, 2H, NH; D_2O exchangeable); 8.74 (*s*, 1H, H_4); 8.52 (*s*, 1H, H_5); 8.13, 8.11 (*s*, 2H, methine-H); 6.50–7.58 (m, 12H, arom. C–H); 4.36 (t, 2H, N–CH_2); 1.76 (m, 2H, CH_2), 1.23 (m, 6H, CH_2), 0.80 (t, 3H, CH_3); ^{13}CNMR: δ 143.91 (alip. CH=N), 134.78, 134.40, 132.09, 129.91, 122.74, 120.72, 114.88, 111.82, 110.23, 43.02 (N–CH_2), 31.21, 28.81, 26.48, 22.39, 14.00 (CH_3); MS: (Mwt.: 689): m/z (%), 689 [M+, (6.67)], 534 (20.34), 368 (67.22), 339 (100%);

Anal. Calcd. for $C_{42}H_{31}N_{11}$ (689.28): C, 73.13; H, 4.53; N, 22.34, Found: C, 73.55; H, 4.61; N, 22.10%.

3-(6-(2-Carboxy-2-cyanovinyl)-9-hexyl-9H-carbazol-3-yl)-2-cyanoacrylic acid [DCA-HC]

N-hexylcarbazole-3,6-dicarbaldehyde 2 (0.30 g, 1 mmol) and the requested cyanoacetic acid (0.17 g, 2 mmol) were dissolved in ethanol (20 ml) in the presence of piperidine (0.3 ml) as a catalyst. Over 6 h, the reaction was well refluxed, the precipitated was collected after cooling through filtration and washed with water to remove excess of cyanoacetic acid and recrystallized from ethanol to afford DCA-HC.

Light-yellow solid; 90% yield; mp: 230–232 °C; IR: ν/cm^{-1}: 3419 (COOH), 3000 (arom. C–H), 2931, 2862 (alip. C–H), 2224 (C≡N), 1688 (C=O), 1578 (C=C), 1485 (C–N); ^{1}H NMR: δ/ppm: 8.79 (*s*, 2H, COOH, D_2O exchangeable); 8.45 (*s*, 1H, H_4); 8.41 (*s*, 1H, H_5); 8.28 (*s*, 2H, methine-H); 7.87 (*d*, 1H, H_7), 7.82 (*d*, 1H, H_1), 7.17–7.79 (m, 2H, arom. C–H); 4.38 (t, 2H, N–CH_2); 1.75 (m, 2H, CH_2), 1.23 (m, 6H, CH_2), 0.77 (t, 3H, CH_3); ^{13}CNMR: δ 164.34 (C=O), 155.22, 144.86, 143.75, 129.38, 129.28, 125.70, 125.55, 124.18, 122.82, 120.82, 117.46 (C≡N), 116.85, 111.60, 100.42, 43.33 (N–CH_2), 31.30, 28.76, 26.33, 22.22, 14.20 (CH_3); MS: (Mwt.: 441): m/z (%), 441 [M+, (35.70)], 397 (17.05), 353 (36.08), 297 (100%); Anal. Calcd. for $C_{26}H_{23}N_3O_4$ (441.17): C, 70.74; H, 5.25; N, 9.52; Found: C, 70.40; H, 5.45; N, 9.30%.

2′-(((9-Hexyl-9H-carbazole-3,6-diyl)bis(methanylylidene))bis(4-oxo-2-thioxothiazoli-din-3-yl-5-ylidene))diacetic acid [DRA-HC]

Dicarbaldehyde derivatives 2 (0.30 g, 1 mmol) and rhodanine-3-acetic acid (0.38 g, 2 mmol) were mixed in acetic acid (10 ml) and ammonium acetate (5 mol%) as a catalyst. Over 5 h, the product combination was heated under reflux, the precipitate evaporated under pressure and dissolved in distilled water. The aqueous solution was then acidified with concentrated HCl, and the product was filtered off and recrystallized from acetic acid to obtain DRA-HC.

Deep-red solid; 85% yield; mp: 170–172 °C; IR: ν/cm^{-1}: 3450 (br. OH), 3054 (arom. C–H), 2928, 2856 (alip. C–H), 1706 (C=O), 1577 (C=C), 1478 (C–N); ^{1}H NMR: δ/ppm: 10.06 (s, 2H, COOH, D_2O exchangeable); 8.86 (*s*, 1H, H_4); 8.48 (*s*, 1H, H_5); 8.46 (*s*, 2H, methine-H); 7.51–8-25 (m, 4H, arom. C–H); 4.70 (*s*, 4H, CH_2COOH); 4.43 (t, 2H, N–CH_2); 1.76 (m, 2H, CH_2), 1.24 (m, 6H, CH_2), 0.8 (t, 3H, CH_3); ^{13}CNMR: δ 193.89 (C=S), 167.72 (C=O-thiazole), 166.92 (C=O-acetic), 149.59, 144.67, 142.64, 142.44, 135.53, 129.67, 127.78, 125.72, 125.23, 123.60, 123.19, 122.48, 121.76, 118.90, 118.61, 111.65, 111.03, 45.75 (CH_2COOH), 43.33 (N–CH_2), 31.06, 28.61, 26.56, 22.43, 14.20 (CH_3); MS: (Mwt.: 653): m/z (%), 653 [M+, (3.69)], 468 (5.05), 479 (36.08), 380 (100%); Anal. Calcd. for $C_{30}H_{27}N_3O_6S_4$ (653.08): C, 55.22; H, 4.88; N, 6.39, Found; C, 54.90; H, 5.01; N, 5.99%.

Fabrication of DSSCs

Double distilled water and acetone were used to clean fluorinated tin oxide (FTO), where FTO is a conductive glass (15–20 Ω cm^{-2}). Thin layer of TiO_2 paste was coated on the FTO glass plates by Doctor Blade technique method, then allowed to dry in air, and heat-treated at 450 °C for 30 min. After cooling the TiO_2 working electrodes to 80 °C [24], it was immersed in dye solutions (4×10^{-5} M in DMF) of DTC-HC, DCA-HC, and DRA-HC and kept at room temperature for 24 h. A platinized counter electrode was formed by depositing Pt thin film on FTO glass substrate using magnetron sputtering instrument (Hummer 8.1, USA) ($P=100$ W RF, $t=2$ min) followed by heating at 450 °C for 30 min [25]. The counter electrode was placed on the top of the dye-coated TiO_2 film, and few drops of electrolyte consisted of 0.5 M LiI, 0.05 M iodine I_2, 3-methoxypropionitrile, and 0.5 M 4-tertbutylate pyridine TBP, which were inserted between the electrodes.

Photovoltaic characterization

The light current–voltage (*J*–*V*) curves of the DSSCs were recorded by using solar simulator device (PET Photo Emission Tech., Inc. USA). AM 1.5 spectrum is provided by the xenon lamp of the solar simulator. Based on the light *J*–*V* characteristics, the efficiency η, V_{OC} open-circuit voltage, J_{SC} short-circuits, and FF fill factor were measured. Under dark illuminations, an electrochemical workstation was used to record electrochemical impedance spectrum (EIS) (AUTOLAB-potentiostat/galvanostat) over a frequency range from 10 to 10^5 Hz with a bias potential of 0.10 V. Nyquist plots were analyzed using the nonlinear fits to a suitable equivalent circuit model that will fit with Nyquist plots with negligible error.

Molecular modeling studies

DFT analyses have been completed in Materials Studio packages [26] using the DMOL3 software [27, 28]. Calculations for DFT semi-core pseudopods (dspp) were created with dual numerical base sets and polarization properties (DNP) [29]. The RPBE model is focused on the (GGA) generalized gradient approximation as the best functional approximation [30].

Results and discussion

Chemistry

Dye molecules have an essential role in DSSCs performance, and the capability of the solar cell in sun power harnessing depends on dye structure. The synthetic routes followed to prepare the target organic dyes are presented in (Scheme 1). According to the reported method, hexyl-carbazole-3,6-dicarbaldehyde (**2**) was developed by 9H-carbazole alkylation and accompanied by Vilsmeier–Haack formylation [22, 23]. In the present study, *N*-hexyl-carbazole-3,6-dicarbaldehyde (**2**) was used as starting material to prepare the target organic dyes (Scheme 1). The starting material (**2**) reacted as a substrate for the corresponding DRA-HC [31] dye with rhodanine-3-acetic acid, and spectral data and elemental analysis confirmed the structure. Due to hydroxyl and carbonyl groups, IR spectroscopy displayed absorption bands at 3450 and 1706 cm^{-1}, respectively, and its ^{1}H NMR spectrum displayed four signals at δ 0.8, 1.24, 1.76 and 4.43 due to hexyl protons and two singlet signals δ 4.70, 10.06 ppm assigned, respectively, to $-CH_2$ and COOH groups. Likewise, the ^{13}CNMR spectrum displayed signals for hexyl group at δ 14.20, 22.43, 26.56, 28.61, 31.06 in addition to 2 CH_2, 2 C=O and C=S groups at δ 43.33, 45.75, 166.92, 167.72, 193.89, respectively. The DCA-HC [32] was obtained through refluxing of (**3**) with cyanoacetic acid in ethanol catalyzed with piperidine. The pattern of its ^{1}H NMR displayed four signals related to hexyl protons at δ 0.77, 1.23, 1.75, 4.38, three signals related to methine-H, aromatic protons and COOH at δ 8.28, 8.41, 8.79 ppm, respectively. ^{13}CNMR spectrum displayed signals for hexyl carbons at δ 14.20, 22.22, 26.33, 26.33, 28.76, 31.30, $N-CH_2$ signal at δ 43.33, aromatic carbon at δ 100.42–155.22, beside C≡N, C=O at δ 117.46, 164.34 ppm, respectively. The $m/z = 441$ is in agreement with the expected chemical formula $C_{26}H_{23}N_3O_4$.

Reaction of dicarbaldehyde (**2**) with phenyl hydrazine and ethanol gave the desired phenylhydrazone derivative (**3**), where the organic dye (DTC-HC) was obtained by electrophilic substitution of phenylhydrazone (**3**) with tetracyanoethylene in DMF and heating under reflux for 8 h.

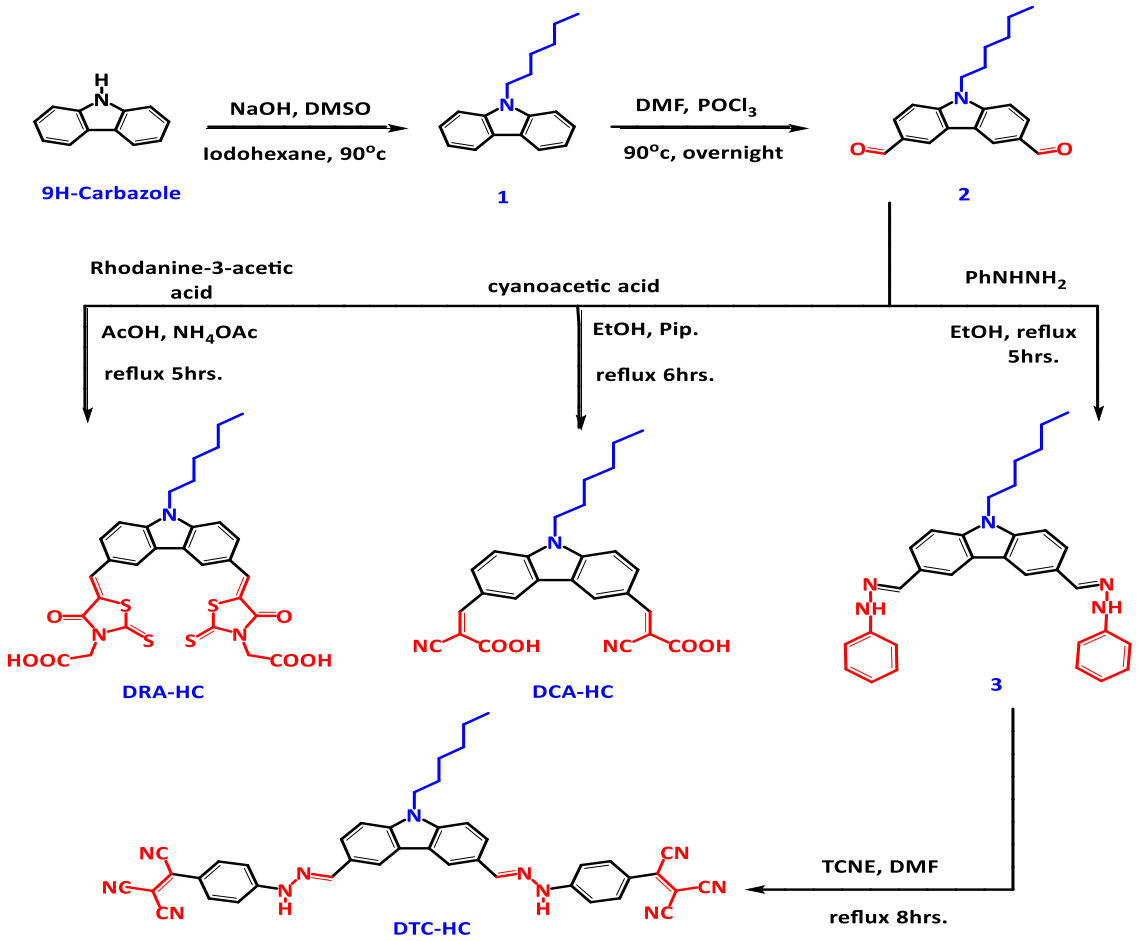

Scheme 1. Synthesis of three required dyes DRA-HC, DCA-HC and DTC-HC

The absorption bands of the IR spectrum were 3319 and 2216 cm^{-1}, respectively, opposite to NH and C≡N groups. The spectrum of ^1H NMR displayed four sharp singlet signals at δ 8.13, 8.11, 8.74, 9.32 ppm specific for the two methine-H, H_4, H_5-carbazole, two NH groups, respectively, multiple signals at δ 6.50–7.58 ppm region owing to aromatic protons. Its mass spectrum showed a molecular ion peak at $m/z = 689$, corresponding to a molecular formula $C_{42}H_{31}N_{11}$.

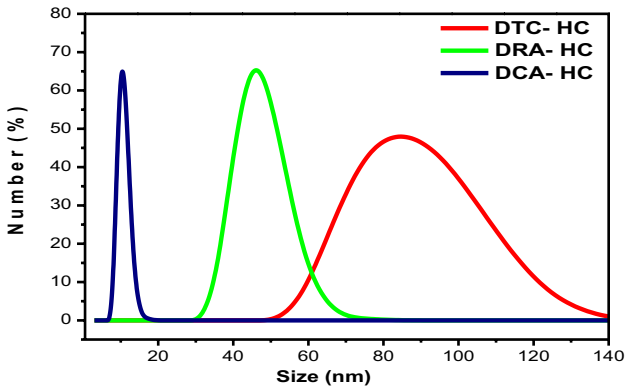

Fig. 2 Particle size distribution of organic dyes

Properties of organic dyes

Particle size analyzer

The particle size distribution of DCA-HC, DRA-HC and DTC-HC dyes were measured and displayed in Fig. 2. The particle sizes of DCA-HC, DRA-HC and DTC-HC were found to be 10 nm, 45 nm and 85 nm, respectively. This indicated all organic dyes are in the range of nanoparticles 1–100 nm. Also, this result is useful in solar cell applications due to increased surface area.

Scanning electron microscope (SEM)

Morphology of organic dyes DCA-HC, DRA-HC and DTC-HC at three different magnifications is shown in Fig. 3). The figure shows that no phase separation in the particle and the homogeneity of the particles can be easily observed. Also, the diameter of particles is small.

Photophysical properties

UV–Vis absorption spectrum of the organic dyes in DMF solution at concentration 4×10^{-5} M is given in Fig. 4, and the corresponding photophysical data are stated in Table 1. The dyes exhibited large absorption spectrums of about 250–500 nm with two absorption bands. At 250–380 nm, short wavelengths can be allocated to the π–π^* transitions of the whole conjugated network, while

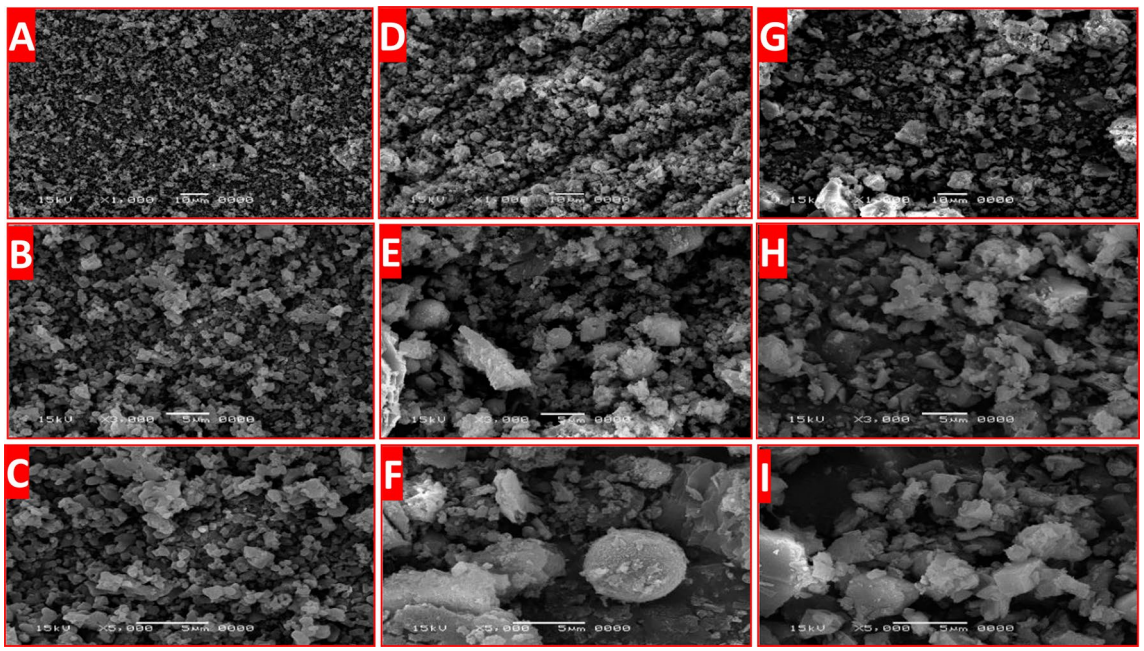

Fig. 3 SEM micrographs surface of DCA-HC at **a** ×1000, **b** ×3000, **c** ×5000, DRA-HC at **d** ×1000, **e** ×3000, **f** ×5000, and DTC-HC at **g** ×1000, **h** ×3000, **I** ×5000

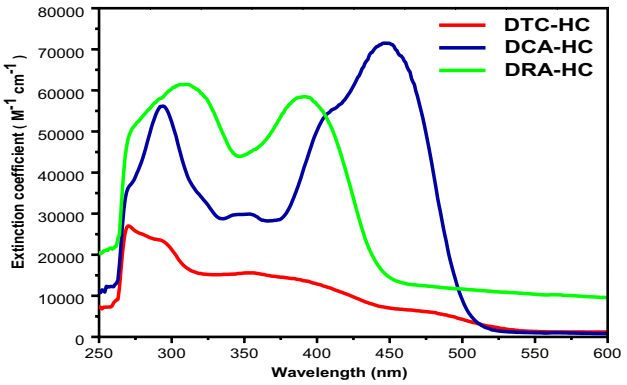

Fig. 4 Absorption spectra of DRA-HC, DCA-HC, and DTC-HC in DMF solution (4×10^{-5} M)

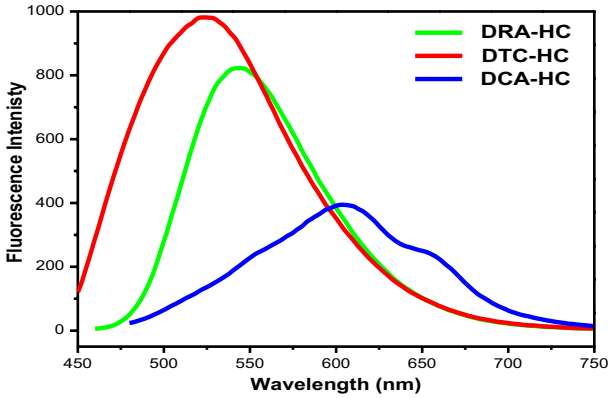

Fig. 5 Fluorescence spectrum of the organic dyes in DMF solution (4×10^{-5} M)

the longer wavelengths between the donor component and the electron drawing part are between 400 and 550 nm, which relate to the ICT. The highest peaks with (λ_{max}) absorption of DCA-HC, DRA-HC and DTC-HC appear at 450, 400 and 395 nm, where the ε (molar absorptivity) values were 7.1×10^4, 5.6×10^4 and 1.4×104 M^{-1} cm^{-1}, respectively, which were higher than those of N3 dyes (1.39×10^4), showing a good light harvest capability. It should be remembered that the presence of rhodanine-3-acetic acid as electron anchoring part into the DRA-HC dye not only leads to peak red absorption, but also improves the ε and expands the spectrum of molecular absorption, which for large photocurrent are highly desirable, due to the presence of C=O and C=S functions which have π–π* and π–π* transitions. But the introduction of cyanoacrylic acid into the DCA-HC dye and tetracyanoethylene into the DTC-HC as electron acceptor unit leads to the absorption peak redshift lower than ε compared to DRA-HC dye. The fluorescence emission distribution of the substances analyzed is also shown in Fig. 5. The λex of DCA-HC, DRA-HC and DTC-HC was 450, 400 and 395 nm, respectively. The maximum emission of DCA-HC, DRA-HC and DTC-HC was 610, 545 and 525 nm, respectively. Emission of three dyes is transferred to the longer wavelength due to the presence of hexyl moiety as electron donor, Emission from DCA-HC is better than the other two dyes; this result could be due to the presence of two cyanoacetic acids anchoring groups.

Electrochemical properties

The cyclic voltammetry (CV) curves given in Fig. 6 and the corresponding data are listed in Table 1. Oxidation potential of three dyes DRA-HC, DCA-HC and DTC-HC *vs* NHE is 0.88, 0.84 and 0.80 V, respectively. It is more positive than the standard potential of iodine/iodide (0.4 vs. NHE) that the photo-oxidized dyes could be expected to be reduced efficiently by the iodine/iodide redox couple. E_{ox} to optical band gap E_{0-0} measured the possible reduction of dyes $E_{0-0}{}^*$ against NHE. From the onset of absorption, the optical band-gap energy was calculated. The $E_{0-0}{}^*$ values measured (−1.57, −1.85, and −1.91 vs. NHE) are more

Table 1 Optical and electrochemical properties of organic dyes in DMF solutions

Dye	[a]λ_{max} (nm)	[a]ε_{max} (M^{-1} cm^{-1})	[b]E_{ox} (V)	[c]HOMO (eV)	[d]LUMO (eV)	[e]E_{0-0} (eV)	[f]$E_{0-0}{}^*$ (V)
DRA-HC	450	68,300	0.88	−5.08	−2.63	2.45	−1.57
DCA-HC	395	56,000	0.84	−5.04	−2.35	2.69	−1.85
DTC-HC	400	31,100	0.80	−5.00	−2.29	2.71	−1.91

[a]Maximum absorption and maximum molar absorption coefficient of dyes in DMF solutions (4×10^{-5} M at 298 K)

[b]Redox potentials are reported with reference to the ferrocene internal standard

[c]Deduced from the oxidation potential using the formula, HOMO = $-(E_{ox}+4.2)$

[d]Obtained from the optical band gap and the electrochemically deduced HOMO value, LUMO = E_{0-0} + HOMO

[e]Band gap E_{0-0}, calculated from the observed optical edge

[f]Excited-state oxidation potential versus NHE

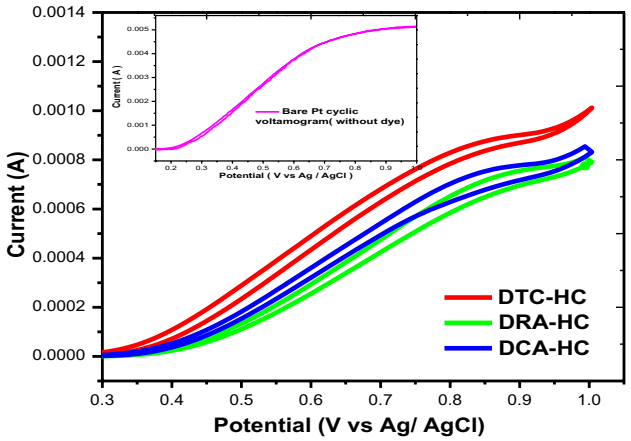

Fig. 6 Cyclic voltammograms of organic dyes recorded and bare Pt cyclic voltammogram blank in DMF solutions (4×10^{-5} M) with TBAI

negative than the TiO_2 conduction band (−0.5 vs. NHE) edge; indication to the cycle of electron injection is powerfully desired to TiO_2, while the dyes are regenerated. As mentioned in Table 1, a negative change between the two E_{ox} and $E_{0-0}{}^{*}$ can be obtained for DTC-HC against DCA-HC by 0.03 V, which led to a similar band gap. Negative changes were found between both E_{ox} and $E_{0-0}{}^{*}$ for DRA-HC against DCA-HC, and it was observed that the E_{ox} shift was greater than that of $E_{0-0}{}^{*}$ which contributed to a decrease in the HOMO–LUMO band gap.

Molecular modeling

Without a crystal structure, to achieve a compound molecular conformation, minimizing energy studies were carried out using DMOL3 calculations based on the DFT semicore pseudopods [27, 28]. Upon geometrical optimization of the synthesized compounds, the molecular parameters are defined in Table 2. The molecular structure of the compounds together with the scheme for atom numeration is shown in Fig. 7.

Molecular parameters

To confirm the study results, theoretical methodology was evaluated to connect the efficiency for the three tested dyes with their electronic properties. It is wanted to estimate the applicability of quantum–mechanical outcomes to investigate the efficiency of such dyes. The quantum outcomes were estimated for the three dyes utilizing the DMOL^3 program. Calculations are used to achieve quantum–chemical specifications of synthesized organic compounds, such as the higher occupied molecular orbital energy (E_{HOMO}), lower unoccupied molecular orbital (E_{LUMO}). Also, the specific parameters, ionization potential (IP), absolute softness (σ), absolute hardness (η), electron affinity (EA), electrophilicity index (ω), maximum amount of electron transfer (ΔN_{max}), separation energy (ΔE), absolute electronegativity (χ), and global softness (S) were measured and calculated [33–37]. In calculations of molecular parameters, Eqs. (1–7) are used as indicated below (Fig. 8):

$$\chi = -1/2\left(E_{LUMO} + E_{HOMO}\right), \tag{1}$$

$$IP = -E_{HOMO}, \tag{2}$$

$$\eta = 1/2\left(E_{LUMO} - E_{HOMO}\right), \tag{3}$$

$$S = 1/2\eta, \tag{4}$$

$$\omega = IP^2/2\eta, \tag{5}$$

$$\Delta N_{max} = -IP/\eta, \tag{6}$$

$$EA = -E_{LUMO}. \tag{7}$$

We can conclude the following from the data obtained in Table 2:

a. The most common quantum–chemical parameters include HOMO and LUMO orbitals. HOMO orbital is the electron donor orbital, it is the highest occupied energy orbital by electrons comprises electrons. LUMO is the electron accepter orbital since it is the lowest energy orbital that can accept electrons. The HOMO and LUMO energies are negative indicating the stability of the synthesized compounds [35].

Table 2 Calculated quantum–chemical parameters of organic dyes

Dye	HOMO	LUMO	x	η	σ	IP	ΔE	ω	ΔN_{max}	EA	S
DRA-HC	−5.01	−3.21	4.11	0.90	1.11	5.01	1.80	13.94	−5.57	3.21	0.45
DCA-HC	−5.17	−3.10	4.14	1.04	0.97	5.17	2.07	12.91	−5.00	3.10	0.52
DTC-HC	−4.55	−3.67	4.11	0.44	2.27	4.55	0.88	23.53	−10.34	3.67	0.22

All units are (eV)

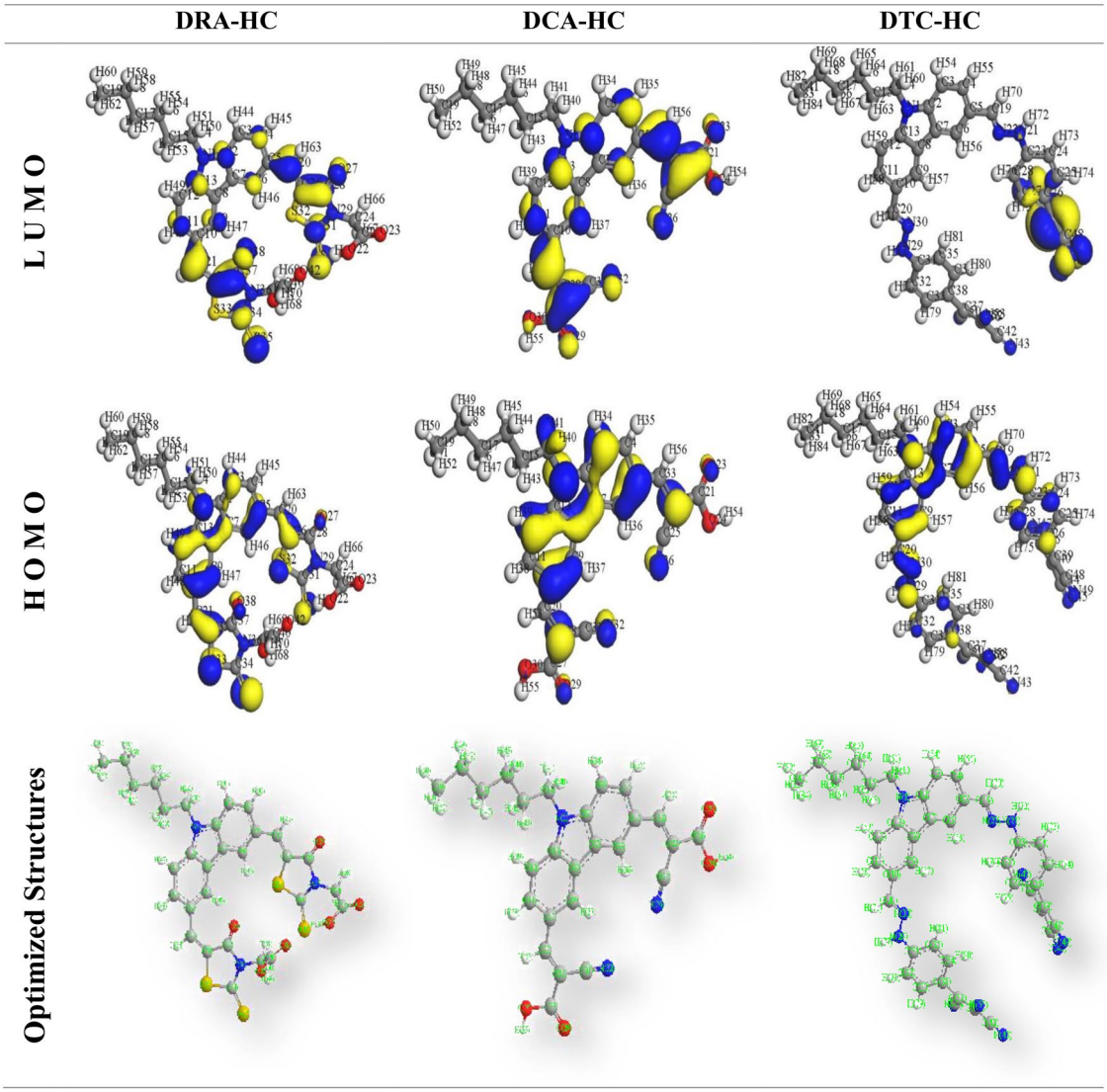

Fig. 7 Electron distributions in the HOMOs and LUMOs and optimized structures of organic dyes

b. Absolute softness (σ) and hardness (η) are essential for the calculation of molecular stability and reactivity. A hard molecule has a large energy gap, while soft molecule has a small energy. The reactivity of soft molecules more than hard molecules may be attributed to their ability to donate electrons to an acceptor more than hard ones.
c. A small HOMO–LUMO gap means a high chemical reactivity [38]. Pearson indicated that energy separation between HOMO–LUMO represents chemical hardness of the molecule [39]. In accordance with the principle of maximum hardness, increased hardness (η) gives the molecule increased stability [40, 41], which is listed in Table 2. The chemical hardness values of compounds are observed in accordance with this order: DCA-HC ($\eta = 1.03$ eV) > DRA-HC ($\eta = 0.90$ eV) > DTC-HC ($\eta = 0.44$ eV).
d. The electrophilicity index (ω) indicates the molecule's ability to accept electrons. The results of this parameter obey this order: DCA-HC ($\omega = 23.53$ eV) > DRA-HC ($\omega = 13.29$ eV) > DTC-HC ($\omega = 12.91$ eV).
e. The energy gap (E_{HOMO}–E_{LUMO}) acts as an important stability index. It can be used as an important parameter for characterization of the chemical molecular reactivity. The soft molecule is a more polarized molecule with a small energy gap.
f. For compound DCA-HC, it was observed that as given in Table 2, It has the highest value of E_{HOMO}, which means the most efficient potential for donated electrons, when the electron removed from its lowest molecular orbital occupation HOMO.

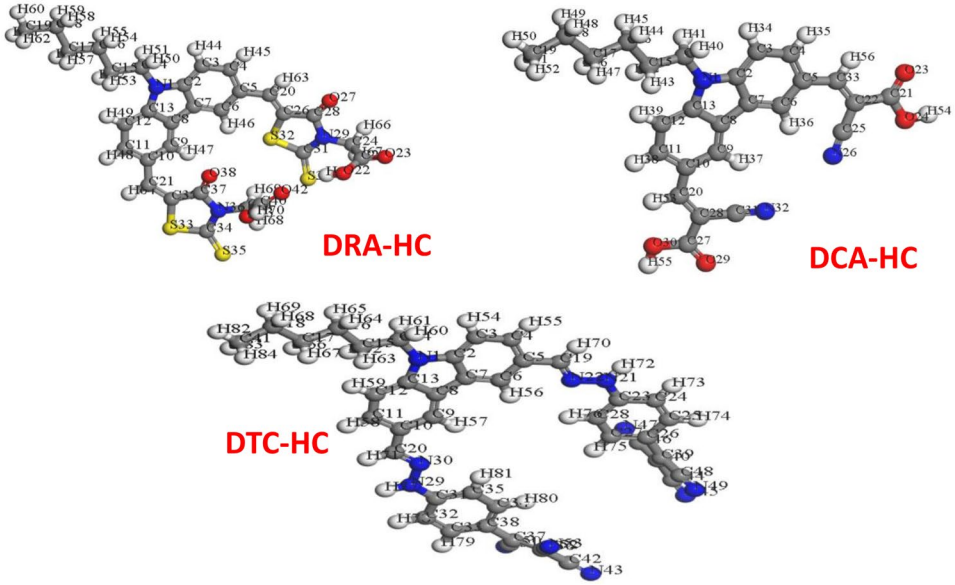

Fig. 8 Out mol geometry optimization of organic dyes by m.s

g. Electron affinity represents the released energy when an electron is added to the smallest unoccupied molecular orbital LUMO. It is higher for DTC-HC (3.67 eV) and lower for DCA-HC (3.10 eV). This confirms that the DTC-HC has a higher tendency to accept an electron to form the anion more than DCA-HC molecule. Thus, DTC-HC dye shows high efficiency as an electron acceptor than DCA-HC. This is confirmed by the lowest hardness and highest dipole moment for DTC-HC, which measures the electrical asymmetry of a molecule.

Photovoltaic performance of DSSCs

Photovoltaic performance of the three organic dyes as sensitizers in DSSCs was calculated by measuring current density–voltage (*J–V*) as shown in Fig. 9, and the corresponding data including short-circuit current (J_{SC}), open-circuit voltage (V_{OC}), fill factor (FF), and photocurrent efficiency or η are mentioned in Table 3. The system focusing on DCA-HC displayed the highest short-circuit current (J_{SC}), compared to the device based on DRA-HC, which exhibits the moderate J_{SC}. The device based on DCA-HC displayed the highest FF (0.81), which gives the highest V_{OC} (0.708 V), P_{max} of (0.354 mW) and highest η (1.41%) due to the highest J_{SC} (2.46 mA/cm^2). The device based on DRA-HC exhibits the

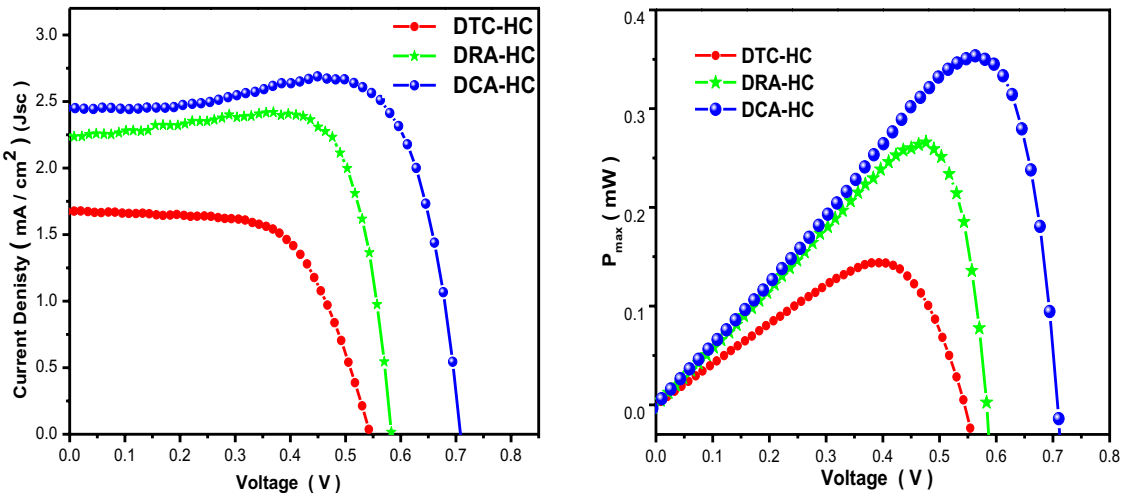

Fig. 9 *J–V* curves and *P–V* curves for the DSSCs of organic dyes. The plots were measured under the light intensity of 1.0 sun

Table 3 Photovoltaic performance of DSSCs based on organic dyes

Dye	V_{OC} (V)	J_{SC} (mA cm^{-2})	FF	η (%)	P_{max} (mW)	[a]R_s (Ω)	[b]R_1 (Ω)	[c]R_2 (Ω)	τ_e (ms)
DTC-HC	0.544	1.67	0.63	0.58	0.143	31.11	5.10	93.78	2.52
DRA-HC	0.583	2.24	0.81	1.06	0.266	30.70	5.60	76.80	2.92
DCA-HC	0.708	2.45	0.81	1.41	0.354	31.30	3.20	46.90	3.37

[a]R_S is FTO interface resistance

[b]R_1 is due to the resistance at the interface between the counter electrode and the electrolyte

[c]R_2 possibly originates from the backward charge transfer from TiO_2 to the electrolyte and the electron conduction in porous TiO_2 film

moderate η (1.06%) and P_{max} of (0.266 mW) due to the moderate I_{SC} (2.24 mA/cm^2), V_{OC} (0.583 V) and FF (0.81). The DTC-HC device exhibits the lowest V_{OC} (0.544 V), the lowest J_{SC} (1.67 mA/cm^2), and moderate FF (0.63) which lead to lowest η (0.58%) and P_{max} of (0.143 mW). The sensitizer has larger energy gap between its LUMO level and the TiO_2 conductive band level with more connected anchor groups, leading to increased electron into TiO_2, increased J_{SC}, and contributing to increase in η percentage. As shown on the chemical structure of the three organic dyes, the electron donating group (D) and conjugating group (π) are the same, but the difference is in the anchoring function. Acrylic acid accepter-based DCA-HC dye is highly efficient among all the dyes in the acceptor modification component. This high efficiency is due to strong electrons withdrawing the character and well-bound acrylic acid in the component dye molecule. In the case of rhodanine-3-acetic acid nucleus-based dyes DRA-HC, the involvement of the –CH_2 group isolates the dye molecules of carboxylic acid, thus preventing the injection of an electron into the TiO_2 conduction band, and this may be the reason for the low performance relative to the acrylic acid. DTC-HC displayed very low efficiency for tetracyanoethylene-based dyes, which could be due to the absence of conjugation between nitrile groups and poor electron-withdrawing dye structure.

Electrochemical impedance spectroscopy (EIS)

EIS is an effective characterization technology in DSSCs of the charge transportation carrier [42]. Usually, high open-circuit voltage (V_{OC}) can also be provided by a large number of electrons in the TiO_2 conduction band. To analyze the comparative charge selection performance with the novel dyes in the DSSC systems, DCA-HC, DRA-HC, and DTC-HC in addition to both the circuit and the Nyquist plot are shown in Fig. 10. Larger semicircles in low-frequency reflect resistance to recombination (R_{rec}) at TiO_2/electrolyte interface. As shown, the radius of the semicircles is increased in this order DTC-HC < DRA-HC < DCA-HC, indicating that the DCA-HC device had the largest resistance between the TiO_2 surface and the electrolyte which can be attributed to the highest voltage obtained.

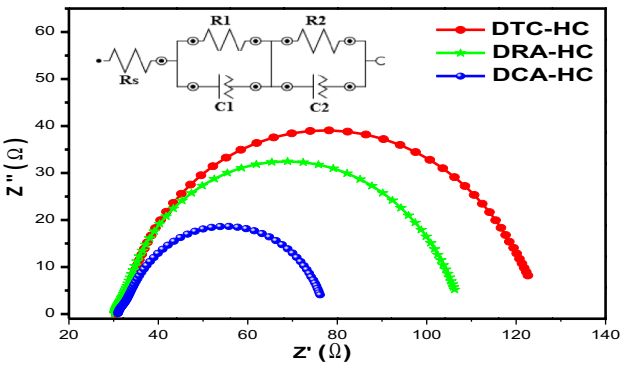

Fig. 10 Nyquist plots for DSSCs based on organic dyes under dark

The results of Nyquist plots are in good agreement with the results of V_{OC} with the DSSCs based on these dyes: DCA-HC (0.708 V) > DRA-HC (0.583 V) > DTC-HC (0.544 V). Also, the major semicircles (R_1) displayed in the Nyquist plots (Fig. 10) of the devices were related to the charge-transfer resistance between the counter electrode and the electrolyte. Also, (R_2) possibly originates from the backward charge transfer from TiO_2 to the electrolyte and the electron conduction in porous TiO_2 film. In this case, Rs value represents the FTO interface and the resistance interface between counter electrode and electrolyte, but we used the same Pt counter electrode and the same electrolyte in our case. The Rs value of all sensitizers, which corresponds to the intercept of the first semicircles in each case, displayed similar results. The results of fitting are listed in Table 3 using the inset model which is simple Randles model including Rs, R with CPE (constant phase element) which is related to nonideal capacitance owing to roughness [43–45]. The electrochemical analysis displayed that the R2 values changed in accordance with applied devices, which the R2 values for sensitizers employing longer branched dyes (93.78 Ω for DTC-HC) were indeed higher than those moderate branched (76.80 Ω for DRA-HC) but decreased in case of simple branched (46.90 Ω for DCA-HC) owing to their increased charge transfer ability. Also, the highest V_{OC} of the device based DCA-HC can be explained by the electron lifetime, calculated through the equation $\tau e = 1/2\pi f$,

where *f* is the peak frequency of lower frequency range in bode plot. The value of τe is listed in Table 3. In order of DTC-HC > DRA-HC > DCA-HC, the lower-frequency peak frequency range is decreased, and the electron recombination lifetime is calculated in reverse with the calculated values of 2.52, 2.92 and 3.37 ms, respectively.

Conclusion

In the present work, three efficient dyes (DTC-HC, DRA-HC, and DCA-HC) with different electron acceptors (tetracyanoethylene, rhodanine acetic acid and cyanoacetic acid) attached to *N*-hexyl carbazole-3,7-dicarbaldehyde (**2**) have been designed and characterized as photosensitizers. The performance of the DSSCs based on the prepared dyes was tested and analyzed. Moreover, introducing the cyanoacetic group as anchoring moiety enhances the TiO_2 conduction band, so the V_{OC} of DCA-HC is higher than other two dyes and the overall conversion power efficiency is increased to 1.41%. Due to the absorption of TiO_2 film and the energy of adsorption, an electron acceptor of dyes including tricyanoethylene group is not sufficient to produce highly efficient solar cells. However, it is suggested that carbazole and alkyl moieties could be applied more than hexyl as a bridge and a donor moiety.

References

1. K. Ranabhat, L. Patrikeev, A. A. Evna Revina, K. Andrianov, V. Lapshinsky, and E. Sofronova, J. Appl. Eng. Sci. **14**, 481 (2016).
2. A. Blakers, N. Zin, K.R. McIntosh, K. Fong, Energy Procedia **33**, 1 (2013)
3. P.A. Troshin, R.N. Lyubovskaya, V.F. Razumov, Nanotechnol. Russ. **3**, 242 (2008)
4. Z. Fan, J. Xiao, K. Sun, L. Chen, Y. Hu, J. Ouyang, K.P. Ong, K. Zeng, J. Wang, J. Phys. Chem. Lett. **6**, 1155 (2015)
5. K.R. Catchpole, A. Polman, Opt. Express **16**, 21793 (2008)
6. T. Sogabe, Q. Shen, K. Yamaguchi, J. Photonics Energy **6**, 040901 (2016)
7. A.N.B. Zulkifili, T. Kento, M. Daiki, A. Fujiki, J. Clean Energy Technol. **3**, 382 (2015)
8. C. Satheeshkumar, M. Ravivarma, P. Rajakumar, R. Ashokkumar, D.C. Jeong, C. Song, Tetrahedron Lett. **56**, 321 (2015)
9. L. Giribabu, V.K. Singh, M. Srinivasu, C.V. Kumar, V.G. Reddy, Y. Soujnya, P.Y. Reddy, J. Chem. Sci. **123**, 371 (2011)
10. M.K. Nazeeruddin, E. Baranoff, M. Grätzel, Sol. Energy **85**, 1172 (2011)
11. W. Wu, J. Wang, Z. Zheng, Y. Hu, J. Jin, Q. Zhang, J. Hua, Sci. Rep. **5**, 8592 (2015)
12. S. Bykkam, B. Kalagadda, V.R. Kalagadda, M. Ahmadipour, C.S. Chakra, V. Rajendar, J. Electron. Mater. **47**, 620 (2018)
13. K. Sharma, V. Sharma, and S. S. Sharma, Nanoscale Res. Lett. **13**, 381 (2018).
14. C.Y. Chen, M. Wang, J.Y. Li, N. Pootrakulchote, L. Alibabaei, C.H. Ngoc-Le, J.D. Decoppet, J.H. Tsai, C. Grätzel, C.G. Wu, S.M. Zakeeruddin, M. Grätzel, ACS Nano **3**, 3103 (2009)
15. S. Mathew, A. Yella, P. Gao, R. Humphry-Baker, B.F.E. Curchod, N. Ashari-Astani, I. Tavernelli, U. Rothlisberger, M.K. Nazeeruddin, M. Grätzel, Nat. Chem. **6**, 242 (2014)
16. L.Q. Bao, P. Ho, R.K. Chitumalla, J. Jang, S. Thogiti, J.H. Kim, Dyes Pigments **149**, 25 (2018)
17. V. Venkatraman, S. Abburu, B.K. Alsberg, Phys. Chem. Chem. Phys. **17**, 27672 (2015)
18. Y. Hua, L.T.L. Lee, C. Zhang, J. Zhao, T. Chen, W.Y. Wong, W.K. Wong, X. Zhu, J. Mater. Chem. A **3**, 13848 (2015)
19. T. Horiuchi, H. Miura, K. Sumioka, S. Uchida, J. Am. Chem. Soc. **126**, 12218 (2004)
20. M. Liang, J. Chen, Chem. Soc. Rev. **42**, 3453 (2013)
21. S.H. Kim, C. Sakong, J.B. Chang, B. Kim, M.J. Ko, D.H. Kim, K.S. Hong, J.P. Kim, Dyes Pigments **97**, 262 (2013)
22. A.S. Beni, M. Zarandi, B. Hosseinzadeh, A.N. Chermahini, J. Mol. Struct. **1164**, 155 (2018)
23. J. Ostrauskaite, V. Voska, J. Antulis, V. Gaidelis, V. Jankauskas, J.V. Grazulevicius, J. Mater. Chem. **12**, 3469 (2002)
24. A.B. Kashyout, M. Soliman, M. Fathy, Renew. Energy **35**, 2914 (2010)
25. D. Kuang, S. Ito, B. Wenger, C. Klein, J.E. Moser, R. Humphry-Baker, S.M. Zakeeruddin, M. Grätzel, J. Am. Chem. Soc. **128**, 4146 (2006)
26. A. Kessi, B. Delley, Int. J. Quantum Chem. **68**, 135 (1998)
27. P.S. Institut, C.-V. Psi, Int. J. **69**, 423 (1998)
28. B. Delley, J. Chem. Phys. **113**, 7756 (2000)
29. Z. Zhang, X. Liu, B.I. Yakobson, W. Guo, J. Am. Chem. Soc. **134**, 19326 (2012)
30. B. Hammer, L.B. Hansen, J.K. Nørskov, Phys. Rev. B Conden. Matter Mater. Phys. **59**, 7413 (1999)
31. T.Y. Wu, M.H. Tsao, S.G. Su, H.P. Wang, Y.C. Lin, F.L. Chen, C.W. Chang, I.W. Sun, J. Braz. Chem. Soc. **22**, 780 (2011)
32. S.A. Kim, H.J. Jo, M.R. Jung, Y.C. Choi, D.K. Lee, M. Lee, J.H. Kim, Mol. Cryst. Liq. Cryst. **551**, 283 (2011)
33. M.K. Nazeeruddin, A. Kay, I. Rodicio, R. Humphry-Baker, E. Müller, P. Liska, N. Vlachopoulos, M. Grätzel, J. Am. Chem. Soc. **115**, 6382 (1993)
34. P. Geerlings, F. De Proft, W. Langenaeker, Chem. Rev. **103**, 1793 (2003)
35. R. G. Parr and R. G. Pearson, J. Am. Chem. Soc. **105**, 7512 (1983)
36. I. Fernández, E. Martínez-Viviente, P.S. Pregosin, Inorg. Chem. **43**, 4555 (2004)
37. A.A. Soliman, M.A. Amin, A.A. El-Sherif, S. Ozdemir, C. Varlikli, C. Zafer, Dyes Pigments **99**, 1056 (2013)
38. J.I. Aihara, J. Phys. Chem. A **103**, 7487 (1999)
39. R.G. Pearson, Coord. Chem. Rev. **100**, 403 (1990)
40. M. Aljahdali, A.A. El-sherif, Inorg. Chim. Acta **407**, 58 (2013)
41. M.H. Helal, M.A. Salem, M.A. Gouda, N.S. Ahmed, A.A. El-Sherif, Spectrochim. Acta Part A Mol. Biomol. Spectrosc. **147**, 73 (2015)
42. G. Zhu, L. Pan, J. Yang, X. Liu, H. Sun, Z. Sun, J. Mater. Chem. **22**, 24326 (2012)
43. F.E.T. Heakal, A.M. Fekry, M.Z. Fatayerji, J. Appl. Electrochem. **39**, 1633 (2009)
44. F. El-Taib Heakal, O.S. Shehata, N.S. Tantawy, A.M. Fekry, Int. J. Hydrog. Energy **37**, 84 (2012)
45. F. El-Taib Heakal, M.M. Hefny, A.M. Abd El-Tawab, Int. J. Electrochem. Sci. **8**, 4610 (2013)